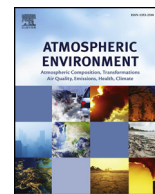




Contents lists available at ScienceDirect

Atmospheric Environment

journal homepage: www.elsevier.com/locate/atmosenv

Modeling the contributions of Northern Hemisphere dust sources to dust outflow from East Asia



Zhiyuan Hu^a, Jianping Huang^{a,*}, Chun Zhao^b, Jiangrong Bi^a, Qinjian Jin^c, Yun Qian^d,
L. Ruby Leung^d, Taichen Feng^a, Siyu Chen^a, Jianmin Ma^a

^a Key Laboratory for Semi-Arid Climate Change of the Ministry of Education, College of Atmospheric Sciences, Lanzhou University, Lanzhou, 730000, China

^b School of Earth and Space Sciences, University of Science and Technology of China, Hefei, Anhui, China

^c Center for Global Change Science, Massachusetts Institute of Technology, Cambridge, MA, USA

^d Atmospheric Sciences and Global Change Division, Pacific Northwest National Laboratory, Richland, WA, USA

ARTICLE INFO

Keywords:

Dust aerosols
Mass flux
Source contribution
Dust number loading
East Asia

ABSTRACT

Mineral dust aerosols can substantially influence the Earth's climate by altering the radiation budget and modifying cloud microphysical and radiative properties. Through long-range transport, dust aerosols could have a global impact. Here, using a fully coupled meteorology-chemistry model (WRF-Chem) and the tracer-tagging technique, we conduct quasi-global simulations to investigate the characteristics of dust intercontinental transport in the Northern Hemisphere and the source contributions to dust outflow from East Asia. Model results show that total dust emission from the main deserts (i.e., North Africa desert (NFD), Middle East desert (MED) and East Asia desert (EAD)) is about 4531 Tg yr^{-1} , in which 66% is from NFD, 24% is from MED and 10% is from EAD. During long-range transport, the NFD and MED dust plumes are separated into two branches by the Tibetan Plateau, with higher dust concentration of $4 \mu\text{g m}^{-3}$ in the northern branch (37° N – 60° N). The imported dust mass from NFD and MED to East Asia is 16.0 Tg yr^{-1} and 33.8 Tg yr^{-1} , respectively; the local dust mass emitted from EAD can circumnavigate and import about 0.41 Tg yr^{-1} of dust into East Asia. As part of the “Asian outflow”, the MED and NFD dust is transported above 600 hPa with concentration of $2 \mu\text{g m}^{-3}$, while the EAD dust is mainly transported below 600 hPa with concentration of $3 \mu\text{g m}^{-3}$. The total outflow dust mass from East Asia is 12.0, 9.7 and 7.7 Tg yr^{-1} from EAD, NFD and MED, respectively. Dust particles dominate the aerosol mass concentration with a fraction of 56.5% in southern East Asia and 75.4% in northern East Asia. Moreover, dust number from EAD dominates the total aerosol number north of 37° N below 600 hPa, with a size range of 0.156 – $0.625 \mu\text{m}$, but the NFD dust number is mainly above 600 hPa. MED dust number dominates the total column aerosol number south of 37° N , with a size range of 0.312 – $0.625 \mu\text{m}$. Quantifying dust source contributions and the associated dust number loading and size distribution over East Asia is important for understanding the role of East Asian dust outflow in climate and hydrological cycle.

1. Introduction

As the second largest contributor (behind sea-salt) to global aerosols by mass, dust aerosols emitted from main deserts such as Sahara, Arabian, Gobi and Taklamakan desert have long lifetime of several weeks (Uno et al., 2009; Yu et al., 2012; Hu et al., 2016; Xu et al., 2018). Therefore, they can be transported thousands of miles from continents and across oceans to affect the weather and climate in downwind regions (e.g., Lau et al., 2008; Yu et al., 2012; Huang et al., 2006, 2014; Zhao et al., 2014; Jin et al., 2014, 2015; Hu et al., 2016). In the atmosphere, dust aerosols can influence the radiation balance directly by absorbing and scattering both solar and terrestrial radiation

(Balkanski et al., 2007; Zhao et al., 2010; Chen et al., 2014). When mixed with clouds, dust aerosols can indirectly affect radiation by modifying cloud micro- and macro-physical properties by acting as cloud condensation nuclei and/or ice nuclei, which also modulate precipitation (Huang et al., 2005, 2006; Creamean et al., 2013; Bi et al., 2017). Near the surface, dust aerosols can dramatically reduce visibility (Chin et al., 2007) and exacerbate air quality (Chin et al., 2007; Huang et al., 2014; Hu et al., 2016), with harmful consequence to human health (Schwartz, 1994; Pope et al., 2002). When deposited on snow/ice surface, dust aerosols accelerate snowmelt and influence the regional hydrological cycle and radiative forcing (Qian et al., 2009; Painter et al., 2010; Huang et al., 2011; Zhao et al., 2014).

* Corresponding author.

E-mail address: hjp@lzu.edu.cn (J. Huang).

<https://doi.org/10.1016/j.atmosenv.2019.01.022>

Received 27 August 2018; Received in revised form 3 January 2019; Accepted 5 January 2019

Available online 21 January 2019

1352-2310/© 2019 Elsevier Ltd. All rights reserved.

Furthermore, deposition of dust aerosols into rainforests and ocean can provide nutrients such as iron and phosphorus to ecosystems, and thus influence carbon cycle and ecosystem evolution (Mahowald et al., 2008; Yu et al., 2015).

Previous studies have revealed that a large amount of dust particles exported from East Asia can reach western North America through trans-Pacific transport and significantly affect the regional energy budget and air quality (Chin et al., 2007; Yu et al., 2012; Hu et al., 2016). Yu et al. (2008, 2012) estimated from satellite observations that about 56 Tg of dust from East Asia reaches the west coast of North America every year. At the ground level, trans-Pacific dust aerosols can bring 3–4 times as many fine particles relative to pollution aerosols to the western US (Chin et al., 2007). Creamean et al. (2013) noted an important role of trans-Pacific transported Saharan and Asian dust aerosols as ice nuclei in orographic precipitation over the western US. However, most studies of dust aerosols over East Asia and their transport are conducted based on cases (Eguchi et al., 2009; Huang et al., 2009), so we lack a climatological view of East Asian dust aerosols and their transport. Furthermore, dust aerosols from North Africa, Middle East, and East Asia have been studied as a single entity known as “Asian outflow” (Chin et al., 2007), but the dust source contributions to the “Asian outflow” are not well understood, leaving large uncertainties in how and why the “Asian outflow” varies from seasonal-to-decadal time scales and they may change in the future.

In this study, a quasi-global simulation following Zhao et al. (2013b) and Hu et al. (2016) is conducted using the Weather Research and Forecasting (WRF) model with chemistry (WRF-Chem; Grell et al., 2005). To understand the dust sources and dust transport over East Asia, the University of Science and Technology of China (USTC) implemented the tracer-tagging method in WRF-Chem to quantify the contributions from different major sources to the dust mass loading over East Asia. We first evaluate the simulation in terms of large-scale circulation and dust mass against reanalysis and satellite datasets, respectively. Then the intercontinental transport characteristics of dust from different source regions, including North Africa, East Asia, North America, and the Middle East, are analyzed, followed by an estimation of the dust mass fluxes from different sources to East Asia. Finally, the dust mass concentration is compared with other aerosol types and their vertical distribution of fractional contributions to the size of dust number loading is analyzed to understand the role of dust aerosols in influencing the regional climate and air pollution over East Asia.

2. Model, experiment design and evaluation data

In this study, the updated WRF-Chem by USTC based on the publicly released version 3.5.1 (Zhao et al., 2013b, 2014; Hu et al., 2016) is used. The MOSAIC (Model for Simulation Aerosol Interactions and Chemistry) aerosol module (Zaveri et al., 2008) is coupled with the CBM-Z (carbon bond mechanism) photochemical mechanism (Zaveri and Peters, 1999). Aerosol size distributions are represented by eight discrete size bins through the bin approach (Fast et al., 2006). Aerosol dynamics implemented in WRF-Chem include emissions, transport (Zhao et al., 2013b), dry and wet deposition (Binkowski and Shankar, 1995; Easter et al., 2004; Chapman et al., 2009), physical and chemical processes (Zaveri et al., 2008). The optical properties and direct radiative forcing of individual aerosol composition are diagnosed following the methodology described in Zhao et al. (2013a). Aerosol-cloud interactions are included in the model following Gustafson et al. (2007) by calculating the aerosol activation and resuspension between dry aerosols and cloud droplets.

The GOCART (Georgia Tech/Goddard Global Ozone Chemistry Aerosol Radiation and Transport) dust emission scheme (Ginoux et al., 2001), which was coupled with MOSAIC in WRF-Chem by Zhao et al. (2010), can improve simulation of vertical dust emission fluxes. Dust particles are emitted into eight size bins with mass fractions of $10^{-6}\%$, $10^{-4}\%$, 0.02%, 0.2%, 1.5%, 6%, 26%, and 45%. Anthropogenic

emissions are obtained from the Hemispheric Transport of Air Pollution version-2 (HTAPv2) at $0.1^\circ \times 0.1^\circ$ horizontal resolution and a monthly temporal resolution for each year of 2010–2015 (Janssens-Maenhout et al., 2015). Biomass burning emissions are obtained from the Fire Inventory from NCAR (FINN) with hourly temporal resolution and 1 km horizontal resolution (Wiedinmyer et al., 2011), and are vertically distributed following the injection heights suggested by Dentener et al. (2006) from the Aerosol Comparison between Observations and Models (AeroCom) project. Sea-salt emission follows Zhao et al. (2013a), which includes correction of particles with radius less than $0.2 \mu\text{m}$ (Gong, 2003) and dependence of sea-salt emission on sea surface temperature (Jaeglé et al., 2011).

Although a global WRF-Chem configuration with only dust aerosols can simulate the dust mass and its radiative forcing (Alizadeh-Chooabari et al., 2014), sophisticated chemistry processes of dust interactions with other aerosols are not currently represented because such simulations cannot run stably due potentially to numerical issues of solving the chemical reactions near the relatively pristine polar regions. Given the need of sophisticated chemistry to simulate both dust and anthropogenic aerosols, a stable quasi-global WRF-Chem configuration is used in this study to circumvent the technical difficulty of global WRF-Chem configuration to characterize the trans-continental transport of aerosols. Our quasi-global channel configuration uses periodic boundary conditions in the zonal direction and includes 360×145 grid cells (180°W – 180°E , 67.5°S – 77.5°N) to perform simulation at 1° horizontal resolution for the period of 2010–2015. The simulation is configured with 35 vertical layers up to 50 hPa. The meteorological initial and lateral boundary conditions are derived from the National Center for Environmental Prediction final analysis (NCEP/FNL) data at 1° horizontal resolution and 6 hourly temporal intervals. The simulated winds and atmospheric temperature are nudged towards the NCEP/FNL reanalysis data throughout the domain with a nudging timescale of 6 h in all cases (Stauffer and Seaman, 1990).

In order to understand the impact of long-range transported dust on regional air quality and weather, this study uses the USTC version of WRF-Chem that applies the tracer-tagging method to quantify the contributions from different major desert regions to the dust loading during the trans-Pacific transport. In this method, dust particles emitted from a number of independent regions with major deserts are tagged and explicitly tracked using additional model variables within a single simulation. Four regions with major deserts globally, i.e., North Africa (0°N – 40°N and 20°W – 35°E), East Asia (25°N – 50°N and 75°E – 150°E), North America (15°N – 50°N and 80°W – 140°W), and elsewhere in the world, are selected as dust source regions in this study. Inside the elsewhere in the world, dust source is dominated by the Middle East (0 – 50°N and 35°E – 75°E) in the Northern Hemisphere (Fig. 2). All the tagged dust variables are treated in the same way as the original dust variable (i.e., physical and advective tendencies are calculated explicitly).

Daily geopotential height, zonal and meridional wind components data sets from ECMWF interim Reanalysis (ERA-interim) ($0.75^\circ \times 0.75^\circ$) (Dee et al., 2011) and Modern-Era Retrospective analysis for Research and Applications (MERRA) ($1/2^\circ \times 2/3^\circ$) (Rienecker et al., 2011) are used to evaluate the model simulation. For aerosol optical depth (AOD), the daily gridded level 3 data sets retrieved by the Moderate Resolution Imaging Spectroradiometer (MODIS) instrument and the Multi-angle Imaging Spectroradiometer (MISR) instrument onboard the Terra spacecraft, which crosses the Equator at local time of $\sim 10:30$ in the morning, are used to evaluate the model results sampled at the same time.

3. Result

3.1. Characteristics of dust intercontinental transport

We first evaluate the simulated geopotential height and AOD

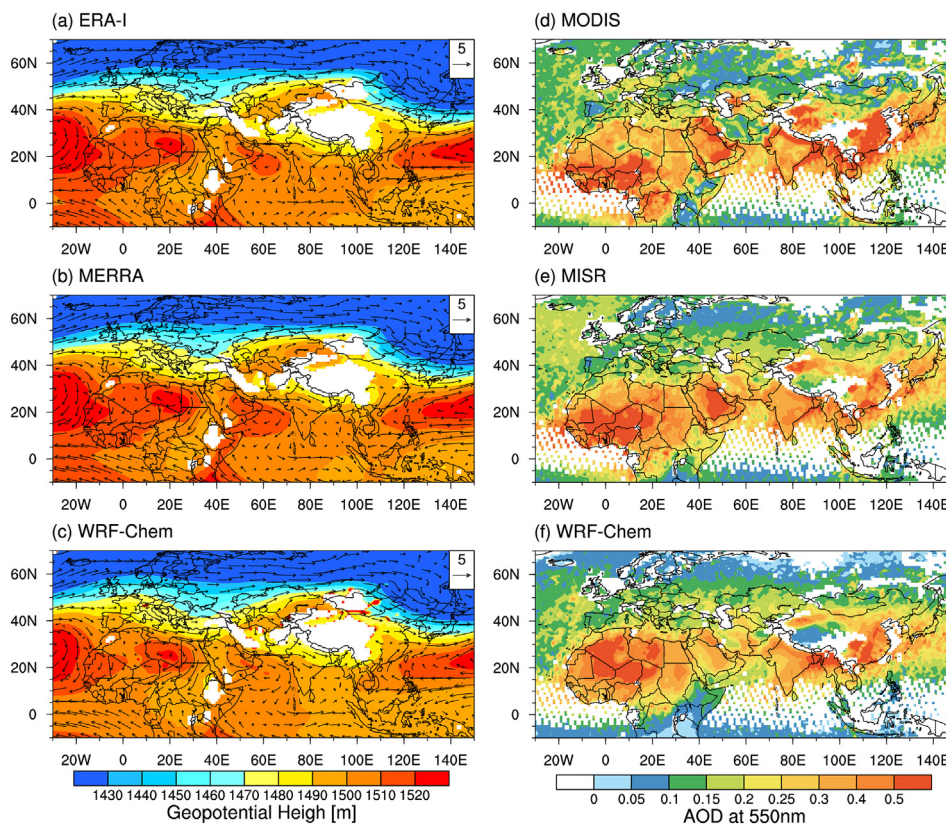


Fig. 1. Seasonal mean geopotential height (shadings; unit: m) and winds (arrows; units: $m s^{-1}$) at 850 hPa from (a) ERA-I, (b) MERRA, and (c) WRF-Chem (Left); and AOD from (d) MODIS, (e) MISR and (f) WRF-Chem (Right) during MAM 2010–2015.

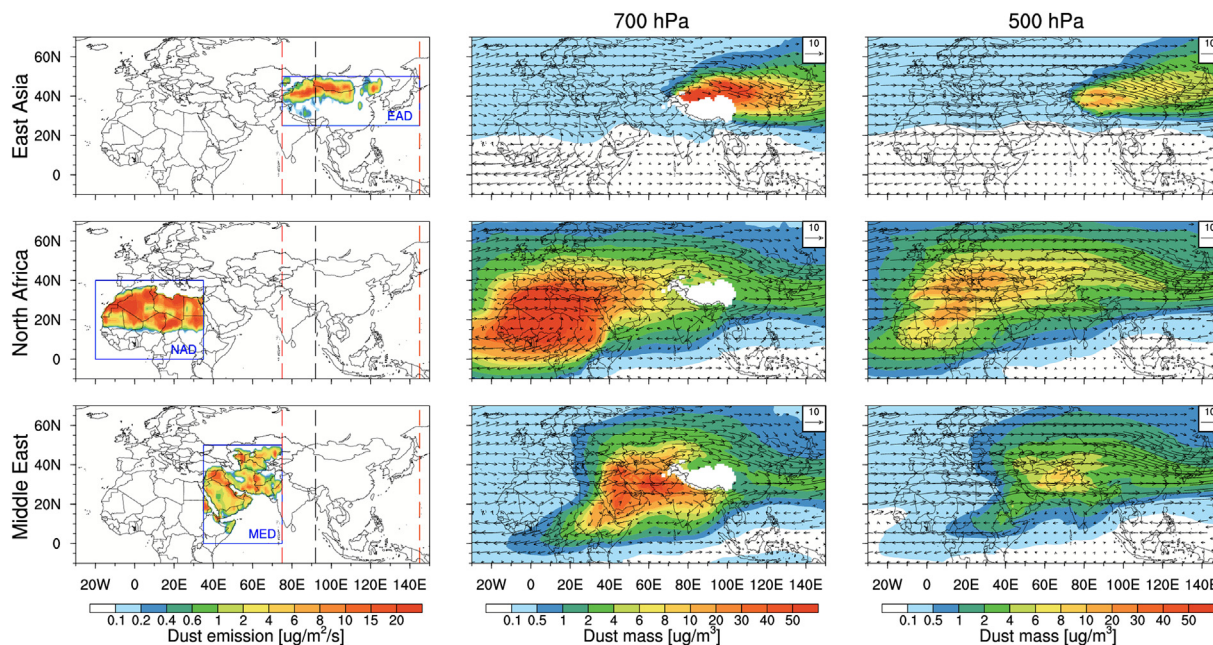


Fig. 2. Spatial distributions of seasonal mean dust emission rate (unit: $\mu g m^{-2} s^{-1}$) over East Asian desert (EAD), North Africa desert (NFD) and Middle East desert (MED) (Left), dust mass concentration (unit: $\mu g m^{-3}$) at 700 hPa (Middle) and 500 hPa (Right) during MAM 2010–2015. In the left panels, the red dotted lines mark $75^{\circ} E$ as the boundary of dust imported into East Asia and $145^{\circ} E$ as the boundary of dust outflow from East Asia. The black dotted line marks $92^{\circ} E$ used as the dividing line between the Gobi and Taklamakan deserts (black dotted line) in East Asia. (For interpretation of the references to colour in this figure legend, the reader is referred to the Web version of this article.)

against the reanalysis data (ERA-interim and MERRA) and the satellite retrieved AOD (MODIS and MISR) for 2010–2015, respectively. Fig. 1 shows that the model can well represent the spatial variability of

geopotential height and winds at 850 hPa over the entire domain in dust active season (spring). Geopotential height and AOD in other seasons are shown in Figs. S1a–c of the supplemental material. The

Model is nudged towards the reanalysis data sets in 6 h intervals, so the geopotential height and winds at 850 hPa can be well represent. More specifically, the model well captures the Northern Hemisphere monsoonal circulations over North Africa, South Asia, and East Asia, which play important roles in transporting dust aerosols horizontally from source regions to remote downwind regions (Uno et al., 2009) and vertically from near surface to troposphere and lower stratosphere (Lau et al., 2018). In order to reduce the sampling discrepancy between simulation and satellite retrievals, the WRF-Chem simulated AOD is sampled and averaged at the same time as the satellite retrievals, and then interpolated to the wavelength of 550 nm using AOD at 400 nm and 600 nm based on the Ångström exponent. Both satellite retrievals and model results show seasonal variability of AOD with the maximum AOD mainly located over North Africa, Middle East, the Thar Desert and Gobi Desert due to dust, as well as in India and South Asia due to anthropogenic aerosols in MAM (Fig. 1 and Figs. S1a–c). However, the MODIS results show a high AOD area at 60° N in JJA (Fig. S1a). This discrepancy could be attributed to the uncertainties in emissions over the regions in model simulations, particle for the biomass burning emissions, where there are lots of forest fire occurs and produce more absorbing aerosols, and biomass burning emission with higher temporal and spatial resolutions are need in future studies (Stocks et al., 1998; Wiedinmyer et al., 2011).

Also, Hu et al. (2016) has used the satellite observational data sets to evaluate the modeling results. It shows that the model simulations can well capture the small-size aerosol over the Asian and western Pacific and represent the seasonal variation of extinction Ångström exponent with observations. Compared with the AAOD derived from OMI, the model can reasonably simulate the decreasing gradient of OMI derived AAOD from the eastern to western of Pacific. However, there are positive (negative) biases in AAOD in the warm (cold) months due to the neglect of the seasonal variability of anthropogenic BC emissions over East Asia. For the extinction profile compared with CALIPSO, the model well captures the seasonality of aerosol extinction profiles with a maximum in MAM, which is largely controlled by the activity of dust outflow events over the Pacific. However, there are difference between the simulation and retrievals in the free troposphere due to the reduced sensitivity of CALIPSO to the aerosol layers above 4 km.

Previous studies have shown that the spatial and seasonal variabilities of absorbing AOD (AAOD) and aerosol size distribution are well represented by WRF-Chem (Zhao et al., 2012, 2013b; Hu et al., 2016). WRF-Chem simulations were used to explore how aerosol trans-Pacific evolution affects the regional climate and surface air quality in western North America (Hu et al., 2016) and the impact of desert dust on the summer monsoon precipitation over southwestern North America (Zhao et al., 2012). Fig. 2 shows the spatial distribution of seasonal mean (2010–2015) dust emission in spring (MAM) and dust mass concentration at 700 hPa and 500 hPa from the WRF-Chem simulation over the desert regions, while the dust emission in other seasons are shown in Fig. 3a–c. Since this study focuses on the dust intercontinental transport over East Asia, we define two meridional boundaries of 75° E and 145° E (red dotted lines in Fig. 2) to quantify the dust aerosols imported into and outflowed from East Asia, respectively. In order to separate the contributions of the Gobi Desert and the Taklamakan Desert to the total dust aerosols in East Asia, we further define 92° E as another meridional boundary (black dotted line in Fig. 2). The model simulates significant amounts of dust emission over the EAD, NFD, and MED (left panels in Fig. 2). The annual total dust emission over the three desert regions is about 4531 Tg (Fig. 6a), which is consistent with the value calculated by Zhao et al. (2012) and approximates to the higher end of the range (3995–4313 Tg yr⁻¹) reported by Huneus et al. (2011). However, this value is about 50% higher than the ~3000 Tg yr⁻¹ estimated by Chin et al. (2009) and Kim et al. (2013) for 2000–2007 using the GOCART model. A potential reason for the discrepancy is the impact of meteorological fields (e.g., surface winds) and land surface conditions (e.g., soil moisture) simulated by

different models that induces different soil erodibility and thus dust emission (Zhao et al., 2012). The different simulation periods could be another reason.

Dust over major deserts (e.g., EAD, NFD and MED) can be lifted to higher altitude by strong frontal and postfrontal convections and turbulent mixing in the boundary layer (Yu et al., 2008). The prevailing westerlies can subsequently transport the elevated dust by thousands of miles to downwind regions (Yu et al., 2008; Hu et al., 2016). Fig. 2 (middle and left columns panels) shows a clear transport pathway of dust from the NFD and MED source regions to East Asia, and these dust merge with the EAD dust as “Asian outflow” dust in MAM, which is transported to North Pacific. The maximum dust mass concentration is seen over the desert regions, with values of more than 50 $\mu\text{g m}^{-3}$ at 700 hPa and 20 $\mu\text{g m}^{-3}$ at 500 hPa. At 700 hPa, the NFD and MED dust are separated into two branches around the Tibetan Plateau. The NFD dust has a concentration of ~6 $\mu\text{g m}^{-3}$ in both the northern and southern branches. However, the MED dust has higher concentrations in south of the Tibetan Plateau than in north of the Tibetan Plateau. This south-north gradient of dust concentration could be attributed to short-distance from source to the Plateau and the blocking effect of high plateau in the south of the Tibetan Plateau (Xu et al., 2018; Jin et al., 2018). At 500 hPa, the maximum outflowed dust is from EAD with a concentration of 8 $\mu\text{g m}^{-3}$, followed by the NFD and MED dust with a concentration of 6 $\mu\text{g m}^{-3}$. Also, we see that high dust mass concentration from EAD is located north of 45° N, while that from NFD and MED is distributed mainly south of 45° N.

To capture the transport characteristics of dust from various deserts, Fig. 3 shows the vertical cross-sections of meridional circulation and zonal dust mass flux over the source regions at 75° E (imported) and 145° E (outflowed) from 0 to 60° N in MAM, which is most significant scenario compared with other seasons (Figs. S3a–c). Clearly, the desert dust can be lifted to 300 hPa or higher with mass concentration decreasing from 40 $\mu\text{g m}^{-3}$ to 1 $\mu\text{g m}^{-3}$. The rising branch of Taklamakan dust is confined between 35 and 45° N, but the Gobi dust has a broader rising branch between 35 and 55° N. When the dust from the two sources merges and outflows from East Asia, the largest mass concentration is located at 900–500 hPa with 6 $\mu\text{g m}^{-3}$ from 40 to 50° N. The NFD dust is imported into East Asia between 25 and 55° N and the MED dust is imported between a much wider range of 3–60° N with a much higher concentration of 40 $\mu\text{g m}^{-3}$ than that of NFD. However, in the outflow region, the NFD dust has a significantly higher dust concentration than the MED dust, because of the MED dust is mainly transported between 0 and 30° N where the Indian summer monsoon rainfall-induced wet-scavenging is most intense (Yu et al., 2008).

Fig. 4 shows the vertical cross-sections of zonal circulation and meridional dust mass flux over 0–37° N (South) and 37° N–60° N (North) from 30° W to 150° E in MAM. Under the prevailing westerlies, the NFD and MED dust are transported eastward to East Asia. During the intercontinental dust transport, dust concentrations are higher in the south than in the north; however, downwind of the source regions (i.e., between 100° E and 145° E), dust concentrations are higher in the north than in the south. This is consistent with Fig. 3 and suggests a significant role of wet removal by the Indian summer monsoon precipitation. The dust outflow in the north is strengthened by the prevailing westerlies above 600 hPa and thus more dust aerosols can reach East Asia, which is consistent with satellite observations from Yu et al. (2012). In East Asia, the dust transport pathway is mainly confined to the north and below 600 hPa, with a concentration of 4 $\mu\text{g m}^{-3}$, which is double that of NFD and MED transported dust. Moreover, there few dust can emit into the upper troposphere due to downdraft wind in DJF and SON (Figs. S4b and 4c) and eastward transport due to the blocked by the east wind in JJA (Fig. S4a).

Fig. 5a and b shows the spatial distributions of seasonal dust dry and wet deposition fluxes from different sources for the period 2010–2015. Clearly, the dry deposition fluxes from different dust sources have larger spatial variability. Over East Asia, the EAD dust dry deposition fluxes

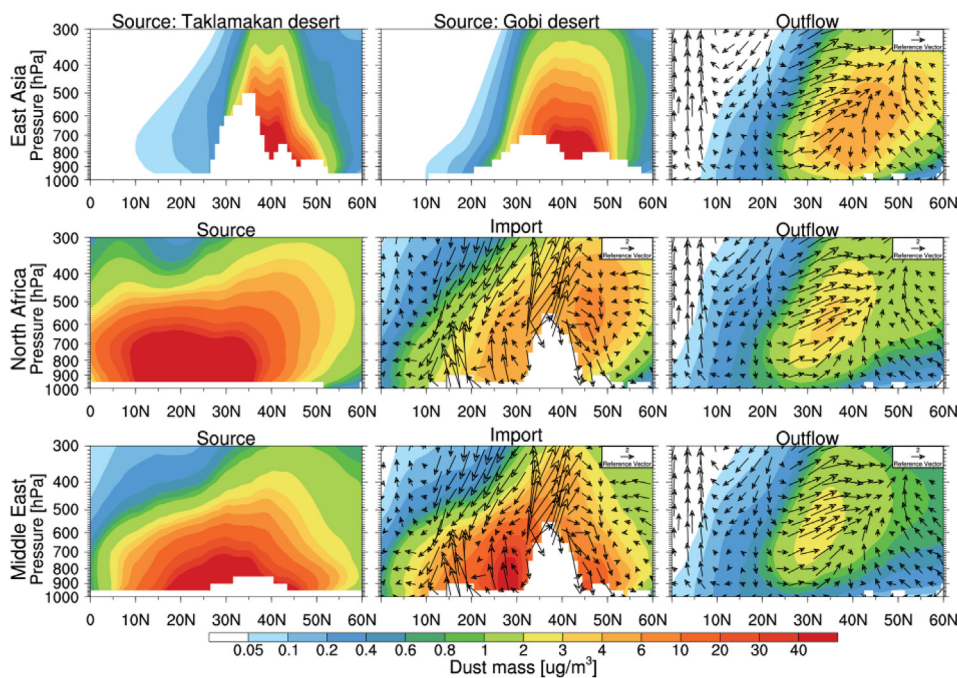


Fig. 3. Vertical cross-sections of zonal dust mass concentration (unit: $\mu\text{g m}^{-3}$) over the source regions in which dust mass concentration (unit: $\mu\text{g m}^{-3}$) from the Taklamakan and Gobi deserts is averaged over $75^\circ\text{E} \sim 92^\circ\text{E}$ and $92^\circ\text{E} \sim 145^\circ\text{E}$, respectively, and Source in North Africa and Middle East is averaged over $20^\circ\text{W} \sim 35^\circ\text{E}$ and $35^\circ\text{E} \sim 75^\circ\text{E}$, respectively; Vertical cross-sections of meridional circulation (unit: m s^{-1}) and zonal dust mass concentration (unit: $\mu\text{g m}^{-3}$) at 75°E (imported) and 145°E (outflow) from 0 to 60°N during MAM 2010–2015.

can reach $\sim 50 \text{ g m}^{-2}$ over the Gobi and Taklamakan desert and nearby regions due to the highest dust mass loading, where the EAD dust contributes more than 60% dry deposition compared with the total deposition (Fig. S6a). Also, the NFD dust and MED dust dry deposition is $\sim 3 \text{ g m}^{-2}$ over north of 40°N with about 5–20% contribution. The dry deposition is determined by dust mass loading, while wet deposition is determined by precipitation and dust mass loading (Zhao et al., 2013b). The wet deposition fluxes have less heterogeneous than that of dry deposition, because of less precipitation over the deserts and less dust mass loading over the regions with more precipitation. Compared with EAD dust wet deposition, NFD dust and MED dust have less wet

deposition over East Asia. In MAM, the dust wet deposition flux can reach about 3 g m^{-2} and decrease 0.3 g m^{-2} when outflow East Asia. Moreover, the EAD dust wet deposition contribution can reach about 50% compared with the total deposition over the south of 40°N , and the wet deposition contribution from NFD and MED dust is about 20% with smaller wet deposition fluxes (Fig. S6b). Overall, the EAD dust dry deposition dominate the total deposition over East Asia, and the EAD dust wet deposition are larger than that from NFD dust and MED dust, especially over the south of 40°N . Furthermore, the NFD dust and MED dust contribute 5–20% dust dry deposition to total deposition over northern East Asia, and 20% dust wet deposition over the southern East

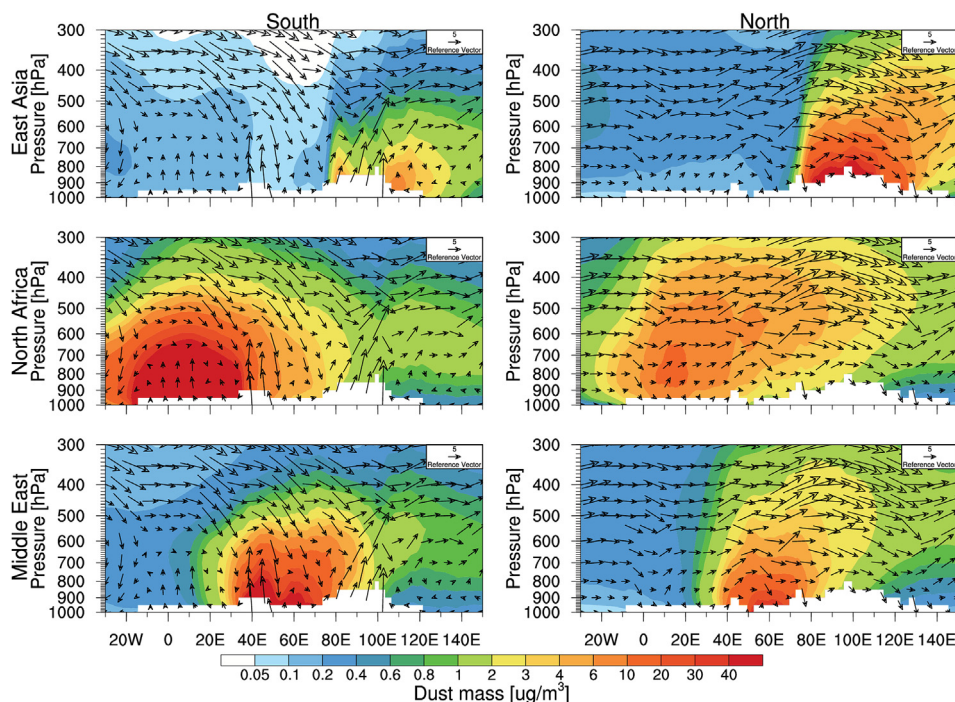


Fig. 4. Vertical cross-sections of zonal circulation (unit: m s^{-1}) and meridional dust mass concentration (unit: $\mu\text{g m}^{-3}$) averaged over $0\text{--}37^\circ\text{N}$ (South) and $37^\circ\text{N} \sim 60^\circ\text{N}$ (North) from 30°W to 150°E during MAM 2010–2015.

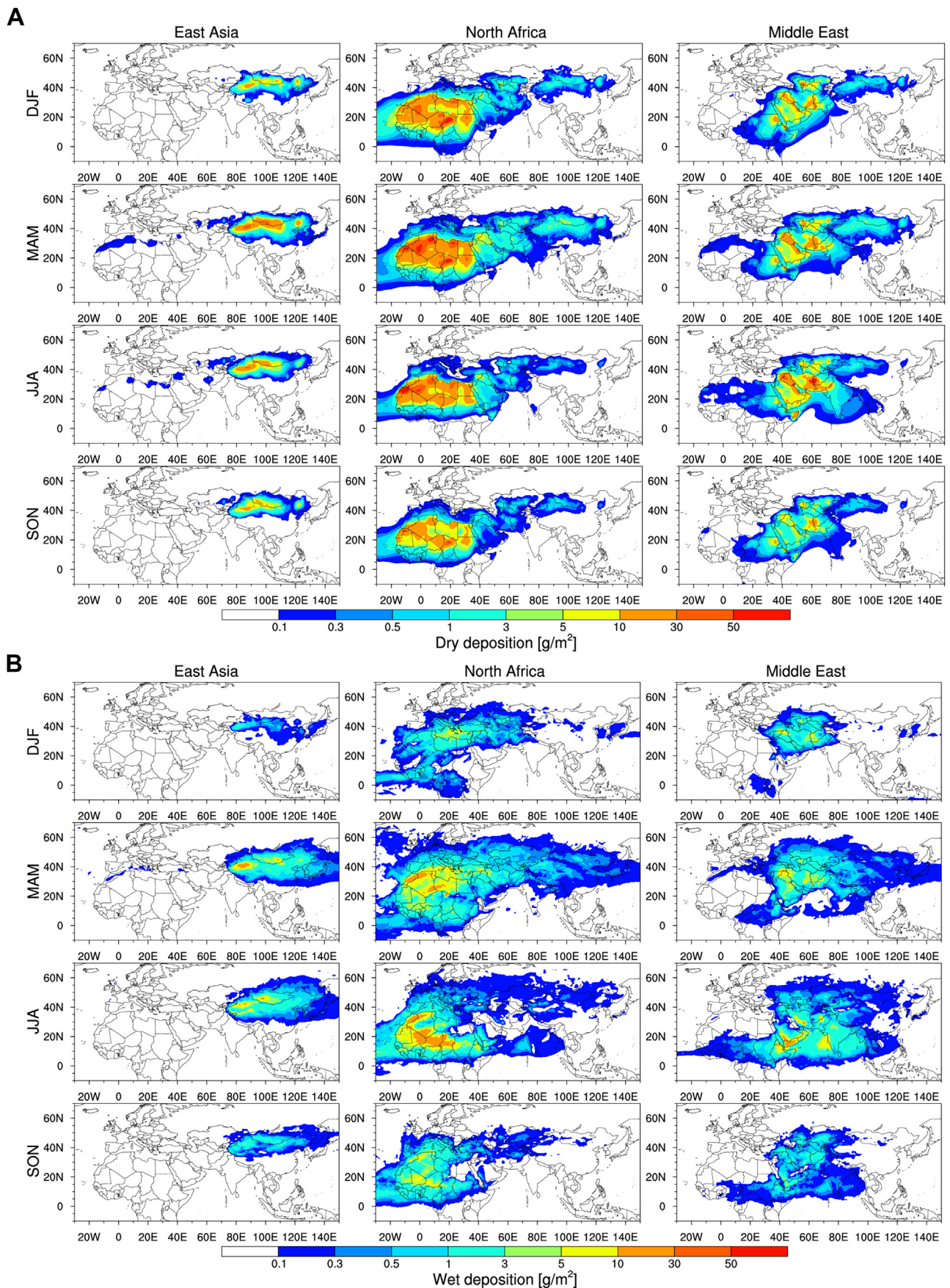


Fig. 5. a. Spatial distributions of seasonal dust deposition fluxes due to dry removal from WRF-Chem simulations in 2010–2015. b. Spatial distributions of seasonal dust deposition fluxes due to wet removal from WRF-Chem simulations in 2010–2015.

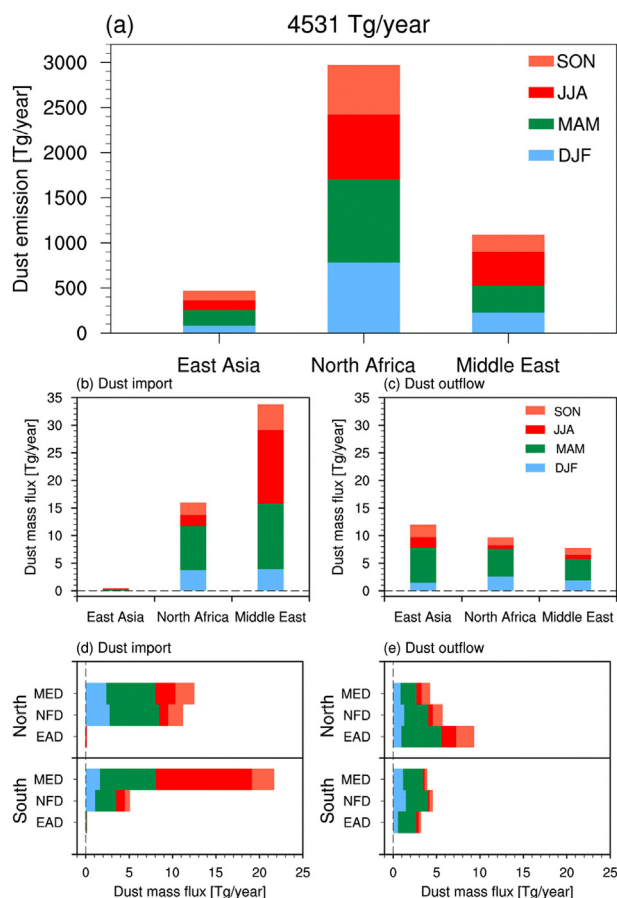


Fig. 6. (a) WRF-Chem estimate of annual mean (2010–2015) dust emission (unit: Tg yr^{-1}) from East Asia, North Africa and Middle East deserts. (b–e) The value of annual global total dust emission (unit: Tg yr^{-1}) is also shown for the import dust mass flux from East Asia, North Africa and Middle East deserts to East Asia (b and d) and the outflow dust mass flux from East Asia originating from East Asia, North Africa and Middle East deserts (c and e). Meridionally integrated dust mass fluxes are shown in (b) and (c) by season, and meridional distributions of seasonal dust mass fluxes are shown in (d) and (e).

Asia.

3.2. Seasonal and latitudinal variations of dust fluxes

As seen in Fig. 2, the elevated desert dust (e.g., NFD and MED) can reach East Asia and merge with the EAD dust and anthropogenic pollution to affect the climate and surface air quality in western North America (Chin et al., 2007; Yu et al., 2012; Hu et al., 2016). Dust emission flux is calculated based on the WRF-Chem simulation (Fig. 6a). On an annual basis, EAD is the smallest dust source with 468 Tg of emitted dust while NFD is the largest dust source with 2973 Tg of emitted dust. For MED, the annual dust emission flux is about 1090 Tg, which is roughly doubled that from EAD. Because of the seasonal variation of extratropical cyclones and the strong mid-latitude westerlies, dust particles emitted from source regions also have a significant seasonal variation (Chin et al., 2007; Yu et al., 2008, 2012; Hu et al., 2016). In spring (MAM), 173 Tg and 920 Tg of dust is emitted from EAD and NFD, respectively, and it's the largest dust emission throughout the entire year. In summer (JJA), the dust emission loading from MED is the largest (about 375 Tg) compared with other seasons. In autumn (SON), the dust emission loading from NFD and MED is smallest with a value of 549 Tg and 189 Tg, respectively. In winter (DJF), EAD has about 83 Tg dust emission loading, which is smallest in all seasons.

The estimate of imported and outflow dust mass with the seasonal

variation is shown in Fig. 6b and c. The annual dust mass imported into East Asia is about 16.0 Tg and 33.8 Tg from NFD and MED, respectively (Fig. 6b). Consistent with the dust emission, the largest dust mass season from NFD is MAM, with a value of 8.0 Tg, which is about 50% of the total annual amount. For MED, the largest dust mass flux season is JJA with a value of 13.3 Tg. However, because of the westerlies, the dust from EAD lofted to the upper troposphere would circumnavigate one full circle around the globe (Uno et al., 2009) and import to East Asia with a value of 0.41 Tg yr^{-1} (Fig. 6b). On the other hand, the largest annual outflow mass flux is from EAD with a value of 12.0 Tg, followed by NFD (9.7 Tg) and MED (7.7 Tg). Compared with the imported mass flux, the outflow values are reduced by 39.4% (NFD) and 77.2% (MED). Across the seasons, the largest outflow occurs in MAM, with dust mass fluxes of 6.4 Tg (EAD), 5.0 Tg (NFD) and 3.9 Tg (MED).

Meridional distributions and seasonal variation of dust mass flux from different sources are shown in Fig. 6d and e. For the dust import, NFD has a higher dust mass flux of 11.2 Tg in the north compared to the south. In contrast, the dust mass flux from MED is larger in the south than the north. Over the north, the maximum dust mass flux season is MAM with a value of 5.7 Tg (NFD) and 5.6 Tg (MED). Over the south, the season of maximum dust mass flux from NFD is MAM with a value of 2.4 Tg, but for the MED the season is JJA (11.1 Tg). For the dust outflow, the largest dust mass flux of 9.3 Tg is from EAD over the north because of the proximity to the source region, followed by NFD (5.7 Tg) and MED (4.2 Tg), and the dust mass flux from EAD, NFD and MED is 3.2 Tg, 4.6 Tg and 3.9 Tg over the south, respectively, with maximum value in MAM.

3.3. Comparison between dust and other aerosol mass and the dust number loading vertical distribution

The vertical distribution of various aerosol compositions (e.g., dust, SO_4 , OM, BC, OM, NO_3 , OIN, NH_4 and sea-salt) are shown in Fig. 7a and b. Four types of dust composition are defined as emitted from NMD (North America desert), EAD, NFD and MED sources in the improved WRF-Chem model. Clearly, the aerosol mass concentration significantly decreases with the altitude in both south and north regions. The maximum dust fraction of about 60% is located between 600 and 400 hPa in the south, in which the fraction of EAD, NFD and MED dust is 18.4%, 16.2% and 22.5% (Fig. 7a). Between 800 and 200 hPa, MED dust contributes more mass concentration fraction (22.3%) than EAD (14.7%) and NFD (14.1%) dust. In the north region, because of the dust source locations (e.g., Gobi and Taklamakan desert), EAD dust can contribute more than 78% to the total aerosol mass below 600 hPa. At 400–600 hPa, EAD dust contributes about 35.0%, followed by NFD dust (23.1%) and MED dust (17.9%). Above 400 hPa, NFD dust becomes the major contributor with a value of 23.2%. Overall, at the height of dominant aerosol transport (600–200 hPa), dust is the major aerosol particle that contributes 56.5% to the total aerosol mass in the south, where the mass concentration of EAD, NFD and MED dust is 0.34 , 0.34 and $0.47 \mu\text{g m}^{-3}$, respectively; in the north, dust contributes 75.4% to the total aerosol mass, where the mass concentration of EAD, NFD and MED dust is 1.46, 1.17 and $0.89 \mu\text{g m}^{-3}$, respectively.

Monthly variation of column-integrated mass of various aerosol compositions for the period of 2010–2015 is illustrated in Fig. 7c, d, e and f. In the south, MED dust is higher than EAD and NFD dust with maximum mass concentration of 16.9 mg m^{-2} in June and minimum mass concentration of 2.4 mg m^{-2} in December, respectively. The maximum mass concentration of EAD and NFD dust is 12.4 mg m^{-2} in May and 10.5 mg m^{-2} in April, respectively, and the minimum mass concentration is 2.7 mg m^{-2} in January and 1.1 mg m^{-2} in August, respectively. Compared with SO_4 and OM, EAD and NFD dust are lower in September–March, but MED dust is higher in April–September. Other aerosols, mainly composed of OM, SO_4 , NO_3 , NH_4 , OIN and sea-salt, have similar total mass concentration compared with dust. Fig. S5 shows the spatial distribution of aerosol component column mass from

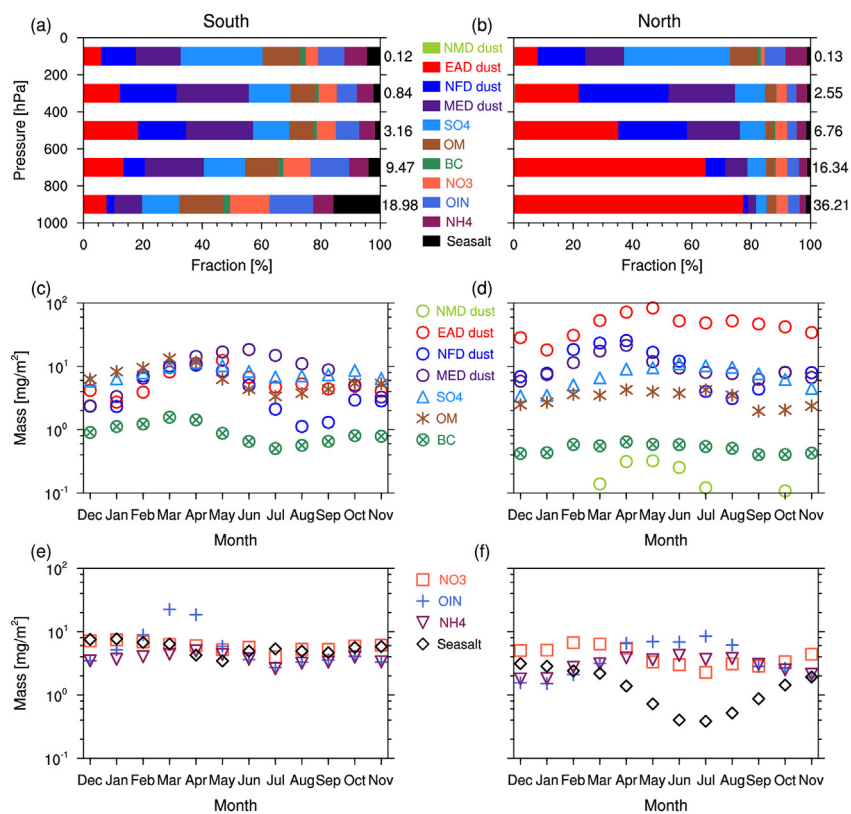


Fig. 7. Fractions of aerosol composition to the total aerosol mass concentration (units: $\mu\text{g m}^{-3}$) in five separate vertical layers: 0–200, 200–400, 400–600, 600–800 and 800–1000 hPa from the WRF-Chem simulation averaged for 2010–2015 in the south (0–37° N; 75° E–145° E) (a) and north (37° N – 60° N; 75° E–145° E) (b). The numbers on the right vertical axis of panels (a) and (b) represent the averaged aerosol mass concentration in the five vertical layers. Monthly mean of aerosol composition column mass concentration (units: $\mu\text{g m}^{-2}$) in the south (c, e) and north (d, f).

WRF-Chem simulations averaged for 2010–2015. Clearly, the OM, SO₄, NO₃ and NH₄ are mainly from the India and eastern China due to the precursor gases emitted from power plants, industries, automobiles, and biomass burning (Chin et al., 2007; Yu et al., 2008; Guttikunda et al., 2014; Hu et al., 2016) and the OIN are mainly from East Asia. Also, the Indian Ocean and Pacific Ocean can produce sea-salt and import into the atmosphere over this region. In the north, EAD dust is the largest aerosol composition with maximum mass concentration of 83.6 mg m^{-2} in May and minimum mass concentration of 18.2 mg m^{-2} in January. NFD and MED dust are comparable with maximum mass concentration of 25.5 mg m^{-2} and 21.4 mg m^{-2} in April. The minimum mass concentration of 3.1 mg m^{-2} (NFD dust) and 5.8 mg m^{-2} (MED dust) is in August and December, respectively. Also, we can see that the mass concentration of NFD and MED dust is smaller than that of SO₄ and OM in June–September.

Dust number concentration is a critical factor in models as it can influence clouds and radiative forcing. Zhao et al. (2013b) examined the uncertainties in modeling dust radiative forcing using three different dust size distribution based on the WRF-Chem model and showed that the MOSAIC aerosol scheme with the 8-bin could well represent the dust size and dust number loading spatial distribution. To better understand the vertical distribution of dust number, the WRF-Chem simulated annual mean (2010–2015) vertical distributions of fractional contributions to the size of dust aerosol number over East Asia is shown in Fig. 8. Here, East Asia is divided into regions south and north of 37° N from 75° E to 145° E. Clearly, the transported dust particles have a dominant size range of 0–2.5 μm , especially between 0.156 and 1.25 μm . The EAD dust number is dominated in the north by a size range of 0.156–0.625 μm below 600 hPa because the dust emission source is located in this region. And we can see that the dust number fraction significantly decreases with the altitude with a maximum value of 14% located at 900–700 hPa. For the NFD dust number, the fraction is mainly in the range of 0.156–0.625 μm above 600 hPa and the maximum value can reach 16% in both north and south regions. Overall, the dust number over East Asia from EAD is mainly transported

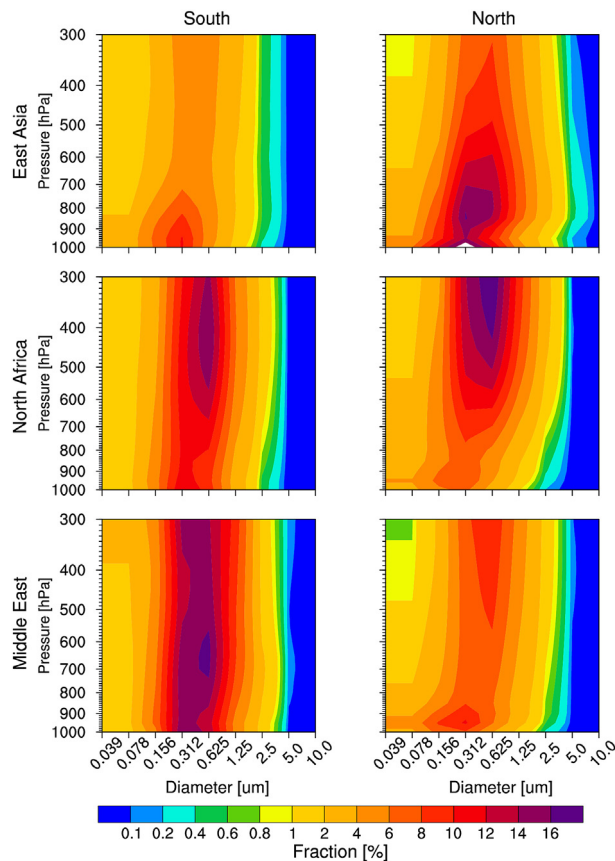


Fig. 8. Vertical distribution of fractional contributions to the particle numbers of dust aerosols for different size bins averaged over 0–37° N (South) and 37° N–60° N (North) between 75° E–145° E. The data sets are averaged between 2010 and 2015.

in the north at a lower altitude, but the EAD dust number has similar value in the south and north at a higher altitude. Different from EAD and NFD dust number, the MED dust number fraction is mainly in the south with a size range of 0.312–0.625 μm in the total column with a value of 16%. This is attributed to the fact that MED dust is mainly transported south of 37° N and the topographic forcing of the Tibetan Plateau can lift the dust particle into the upper troposphere (Xu et al., 2018).

4. Conclusions and discussion

In this study, a fully coupled meteorology-chemistry model (WRF-Chem) is configured to conduct quasi-global simulation for 6 years (2010–2015). In order to better characterize the dust source contribution over East Asia, the tracer-tagging technique developed by Wang et al. (2014) is employed in the dust aerosol simulation to characterize the dust particles emitted from three major desert regions (NFD, EAD, and MED). We use reanalysis data (ERA-interim and MERRA) and the satellite retrieved AOD (MODIS and MISR) to evaluate the model performance in simulating the spatial patterns of geopotential height and AOD. Model results indicate that the total dust emission loading over the three desert regions is about 4531 Tg yr^{-1} . Prevailing westerlies transport the dust from NFD and MED eastward and then they merge with the EAD dust. Over the desert regions, the maximum dust mass concentration can reach more than 50 $\mu\text{g m}^{-3}$ at 700 hPa and 8 $\mu\text{g m}^{-3}$ at 500 hPa. During intercontinental transport, the NFD and MED dust are divided into two branches by the Tibetan Plateau with a higher value of 4 $\mu\text{g m}^{-3}$ over the north. The NFD dust aerosols are transported into East Asia mainly between 25° N–55° N and the MED dust aerosols are transported between 3° N–60° N. However, less MED dust aerosols are transported south of the Tibetan Plateau because of stronger wet scavenging in this region (Yu et al., 2008). For the outflow, the EAD dust is mainly located below 600 hPa with a value of 3 $\mu\text{g m}^{-3}$, and the MED and NFD dust is mainly above 600 hPa with a value of 2 $\mu\text{g m}^{-3}$.

On an annual basis, NFD has a maximum dust loading of 2973 Tg yr^{-1} , followed by MED with a value of about 1090 Tg yr^{-1} , and EAD has a minimum dust emission loading of 468 Tg yr^{-1} . There are about 16.0 Tg yr^{-1} and 33.8 Tg yr^{-1} of dust from NFD and MED imported into East Asia and about 12.0 Tg yr^{-1} of EAD dust is outflow from East Asia. For the outflow, and the dust mass flux is 6.4 Tg yr^{-1} for EAD, 5.0 Tg yr^{-1} for NFD and 3.9 Tg yr^{-1} for MED with the largest outflow in spring.

Dust aerosols are the most dominant aerosol composition by mass over land. In the south region, dust aerosols contribute 56.5% to the total aerosol mass concentration, in which EAD dust, NFD dust, MED dust is 0.34, 0.34 and 0.47 $\mu\text{g m}^{-3}$, respectively. In the north region, because of EAD dust, the dust contribution reaches 75.4% with 1.46 $\mu\text{g m}^{-3}$ of EAD dust, 1.17 $\mu\text{g m}^{-3}$ of NFD dust and 0.89 $\mu\text{g m}^{-3}$ of MED dust. In general, the maximum dust mass concentration of 12.4 (EAD dust), 10.5 (NFD dust) and 16.9 (MED dust) mg m^{-2} is in June, May and April, respectively. The dust number from EAD is mainly in the north with a size range of 0.156–0.625 μm below 600 hPa. For the NFD dust number, the fraction is mainly in a similar particle size range above 600 hPa with the maximum value of 16%. However, the MED dust number fraction is mainly in the south with a size range of 0.312–0.625 μm in the total column with the fraction of 16%.

Our findings show that the NFD dust and MED dust can be transported into South and East Asia following the prevailing westerlies and merge with the EAD dust, and subsequently transported to North Pacific. These dust aerosols can reach mid-to-upper troposphere during their long-range transport (Figs. 3 and 4) and could provide an important source of ice nuclei and influence the cloud radiative forcing. Such impacts of dust aerosols over East Asia and North Pacific are understudied and should be addressed in future studies.

Acknowledgements

This research was supported by the Foundation for National Natural Science Foundation of China (No. 41805116), Innovative Research Groups of the National Science Foundation of China (grant no. 41521004) and the Strategic Priority Research Program of Chinese Academy of Sciences, (Grant No. XDA20060103). Chun Zhao is supported by the “Thousand Talents Plan for Young Professionals” program, the Fundamental Research Funds for the Central Universities, and the National Natural Science Foundation of China NSFC (Grant No. 41775146) of China. Jianrong Bi is supported by the Fundamental Research Funds for the Central Universities lzujbky-2017-56, lzujbky-2017-kb14 and lzujbky-2018-k04. Yun Qian and L. Ruby Leung are supported by Office of Science, U.S. Department of Energy Biological and Environmental Research, through the Regional and Global Climate Modeling program. PNNL is operated by Battelle Memorial Institute for the U.S. Department of Energy under contract DE-AC06-76RLO-1830.

Appendix A. Supplementary data

Supplementary data to this article can be found online at <https://doi.org/10.1016/j.atmosenv.2019.01.022>.

References

- Alizadeh-Choobari, O., Zawar-Reza, P., Sturman, A., 2014. The global distribution of mineral dust and its impacts on the climate system: a review. *Atmos. Res.* 138, 152–165.
- Balkanski, Y., Schulz, M., Claquin, T., Guibert, S., 2007. Reevaluation of Mineral aerosol radiative forcings suggests a better agreement with satellite and AERONET data. *Atmos. Chem. Phys.* 7, 81–95.
- Bi, J., Huang, J., Shi, J., Hu, Z., Zhou, T., Zhang, G., Huang, Z., Wang, X., Jin, H., 2017. Measurement of scattering and absorption properties of dust aerosol in a Gobi farmland region of northwestern China - a potential anthropogenic influence. *Atmos. Chem. Phys.* 17, 7775–7792.
- Binkowski, F.S., Shankar, U., 1995. The regional particulate matter model 1. Model description and preliminary results. *J. Geophys. Res.* 100, 26191–26209.
- Chen, S., Zhao, C., Qian, Y., Leung, L.R., Huang, J., Huang, Z., Bi, J., Zhang, W., Shi, J., Yang, L., Li, D., Li, J., 2014. Regional modeling of dust mass balance and radiative forcing over East Asia using WRF-chem. *Aeolian Res.* 15, 15–30.
- Chapman, E.G., Gustafson Jr., W.I., Easter, R.C., Barnard, J.C., Ghan, S.J., Pekour, M.S., Fas, t.J.D., 2009. Coupling aerosol cloud-radiative processes in the WRF-Chem model: Investigating the radiative impact of elevated point sources. *Atmos. Chem. Phys.* 9, 945–964.
- Chin, M., Diehl, T., Ginoux, P., Malm, W., 2007. Intercontinental transport of pollution and dust aerosols: implications for regional air quality. *Atmos. Chem. Phys.* 7, 5501–5517.
- Chin, M., Diehl, T., Dubovik, O., Eck, T.F., Holben, B.N., Sinyuk, A., Streets, D.G., 2009. Light absorption by pollution, dust, and biomass burning aerosols: a global model study and evaluation with AERONET measurements. *Ann. Geophys.* 27, 3439–3464. <https://doi.org/10.5194/angeo-27-3439-2009>.
- Creamean, J.M., Suski, K.J., Rosenfeld, D., Cazorla, A., DeMott, P.J., Sullivan, R.C., White, A.B., Ralph, F.M., Minnis, P., Comstock, J.M., Tomlinson, J.M., Prather, K.A., 2013. Dust and biological aerosols from the Sahara and Asia influence precipitation in the western US. *Science* 339, 1572.
- Dee, D.P., Uppala, S.M., Simmons, A.J., Berrisford, P., Poli, P., Kobayashi, S., Andrae, U., Balmasada, M.A., Balsamo, G., Bauer, P., Bechtold, P., Beljaars, A.C.M., van de Berg, L., Bidlot, J., Bormann, N., Delsol, C., Dragani, R., Fuentes, M., Geer, A.J., Haimberger, L., Healy, S.B., Hersbach, H., Hólm, E.V., Isaksen, I., Kallberg, P., Kohler, M., Matricardi, M., McNally, A.P., Monge-Sanz, B.M., Morcrette, J.J., Park, B.K., Peubey, C., Rosnay, P., de Tavolato, C., Thépaut, J.N., Vitart, F., 2011. The ERAInterim reanalysis: configuration and performance of the data assimilation system. *Q. J. Roy. Meteorol. Soc.* 137, 553–597.
- Dentener, F., Kinne, S., Bond, T., Boucher, O., Cofala, J., Generoso, S., Ginoux, P., Gong, S., Hoelzemann, J.J., Tio, A., Marelli, L., Penner, J.E., Putaud, J.-P., Textor, C., Mchulz, M., van der Werf, G.R., Wilson, J., 2006. Emissions of primary aerosol and precursor gases in the years 2000 and 1750 prescribed data-sets for AeroCom. *Atmos. Chem. Phys.* 6, 4321–4344.
- Easter, R.C., Ghan, S.J., Zhang, Y., Saylor, R.D., Chapman, E.G., Laulainen, N.S., Abdul-Razzak, H., Leung, L.R., Bian, X., Zaveri, R.A., 2004. MIRAGE: model description and evaluation of aerosols and trace gases. *J. Geophys. Res.* 109, D20210. <https://doi.org/10.1029/2004JD004571>.
- Eguchi, K., Uno, I., Yumimoto, K., Takemura, T., Shimizu, A., Sugimoto, N., Liu, Z., 2009. Trans-pacific dust transport: integrated analysis of NASA/CALIPSO and a global aerosol transport model. *Atmos. Chem. Phys.* 9, 3137–3145.
- Fast, J.D., Gustafson, W.I., Easter, R.C., Zaveri, R.A., Barnard, J.C., Chapman, E.G., Grell, G.A., Peckham, S.E., 2006. Evolution of ozone, particulates, and aerosol direct radiative forcing in the vicinity of Houston using a fully coupled meteorology

- chemistry-aerosol model. *J. Geophys. Res.* 111, D21305.
- Ginoux, P., Chin, M., Tegen, I., Prospero, J.M., Holben, B., Dubovik, O., Lin, S.J., 2001. Sources and distributions of dust aerosols simulated with the GOCART model. *J. Geophys. Res.* 106, 20255–20273.
- Gong, S.L., 2003. A parameterization of sea-salt aerosol source function for sub- and super-micron particles. *Glob. Biogeochem. Cycles* 17, 1097.
- Grell, G.A., Peckham, S.E., Schmitz, R., McKeen, S.A., Frost, G., Skamarock, W.C., Eder, B., 2005. Fully coupled “online” chemistry within the WRF model. *Atmos. Environ.* 39, 6957–6976.
- Gustafson, W.I., Chapman, E.G., Ghan, S.J., Easter, R.C., Fast, J.D., 2007. Impact on modeled cloud characteristics due to simplified treatment of uniform cloud condensation nuclei during NEAQS 2004. *Geophys. Res. Lett.* 34, L19809.
- Guttikunda, S., Goel, R., Pant, P., 2014. Nature of air pollution, emission sources, and management in the Indian cities. *Environ. Res.* 95, 501–510.
- Hu, Z., Zhao, C., Huang, J., Leung, L.R., Qian, Y., Yu, H., Huang, L., Kalashnikova, O.V., 2016. Trans-Pacific transport and evolution of aerosols: evaluation of quasi-global WRF-Chem simulation with multiple observations. *Geosci. Model Dev. (GMD)* 9, 1725–1746.
- Huang, J., Minnis, P., Lin, B., Yi, Y., Khaiyer, M.M., Arduini, R.F., Fan, A., Mace, G.G., 2005. Advanced retrievals of multilayered cloud properties using multispectral measurements. *J. Geophys. Res.* 110, D15S18.
- Huang, J., Lin, B., Minnis, P., Wang, T., Wang, X., Hu, Y., Yi, Y., Ayers, J., 2006. Satellite-based assessment of possible dust aerosols semi-direct effect on cloud water path over East Asia. *Geophys. Res. Lett.* 33, L19802.
- Huang, J., Fu, Q., Su, J., Tang, Q., Minnis, P., Hu, Y., Yi, Y., Zhao, Q., 2009. Taklimakan dust aerosol radiative heating derived from CALIPSO observations using the Fu-Liou radiation model with CERES constraints. *Atmos. Chem. Phys.* 9, 4011–4021.
- Huang, J., Fu, Q., Zhang, W., Wang, X., Zhang, R., Ye, H., Warren, S., 2011. Dust and black carbon in seasonal snow across northern China. *Bull. Am. Meteorol. Soc.* 92, 175–181.
- Huang, J., Wang, T., Wang, W., Li, Z., Yan, H., 2014. Climate effects of dust aerosols over East Asian arid and semiarid regions. *J. Geophys. Res. Atmos.* 119, 11398–11416. <https://doi.org/10.1002/2014JD021796>.
- Huneus, N., Schulz, M., Balkanski, Y., Griesfeller, J., Prospero, J., Kinne, S., Bauer, S., Boucher, O., Chin, M., Dentener, F., Diehl, T., Easter, R., Fillmore, D., Ghan, S., Ginoux, P., Grini, A., Horowitz, L., Koch, D., Krol, M.C., Landing, W., Liu, X., Mahowald, N., Miller, R., Morcrette, J.-J., Myhre, G., Penner, J., Perlwitz, J., Stier, P., Takemura, T., Zender, C.S., 2011. Global dust model intercomparison in AeroCom phase I. *Atmos. Chem. Phys.* 11, 7781–7816. <https://doi.org/10.5194/acp-11-7781-2011>.
- Jaeglé, L., Quinn, P.K., Bates, T.S., Alexander, B., Lin, J.T., 2011. Global distribution of sea salt aerosols: new constraints from in situ and remote sensing observations. *Atmos. Chem. Phys.* 11, 3137–3157.
- Janssens-Maenhout, G., Crippa, M., Guizzardi, D., Dentener, F., Muntean, M., Pouliot, G., Keating, T., Zhang, Q., Kurokawa, J., Wankmüller, R., Denier van der Gon, H., Kuenen, J.J.P., Klimont, Z., Frost, G., Darras, S., Koffi, B., Li, M., 2015. HTAP_v2.2: a mosaic of regional and global emission grid maps for 2008 and 2010 to study hemispheric transport of air pollution. *Atmos. Chem. Phys.* 15, 11411–11432. <https://doi.org/10.5194/acp-15-11411-2015>.
- Jin, Q., Wei, J., Yang, Z.L., 2014. Positive response of Indian summer rainfall to Middle East dust. *Geophys. Res. Lett.* 41, 4068–4074. <https://doi.org/10.1002/2014GL059980>.
- Jin, Q., Wei, J., Yang, Z.L., Pu, B., Huang, J., 2015. Consistent response of Indian summer monsoon to Middle East dust in observations and simulations. *Atmos. Chem. Phys.* 15, 9897–9915. <https://doi.org/10.5194/acp-15-9897-2015>.
- Jin, Q., Wei, J., Pu, B., Yang, Z.L., Parajuli, S.P., 2018. High summertime aerosol loadings over the Arabian sea and their transport pathways. *J. Geophys. Res. Atmos. Available: https://doi.org/10.1029/2018JD028588*.
- Kim, D., Chin, M., Bian, H., Tan, Q., Brown, M.E., Zheng, T., You, R., Diehl, T., Ginoux, P., Kucsera, T., 2013. The effect of the dynamic surface bareness on dust source function, emission, and distribution. *J. Geophys. Res.* 118, 1–16. <https://doi.org/10.1029/2012JD017907>.
- Lau, K., Ramanathan, V., Wu, G.X., Li, Z., Tsay, S.C., Hsu, C., Sikka, R., Holben, B., Lu, D., Tartari, G., Chin, M., Koudelova, P., Chen, H., Ma, Y., Huang, J., Taniguchi, K., Zhang, R., 2008. The joint aerosol-monsoon experiment: a new challenge for monsoon climate research. *Bull. Am. Meteorol. Soc.* 89, 369–383.
- Lau, W., Yuan, C., Li, Z., 2018. Origin, maintenance and variability of the Asian tropopause aerosol layer (ATAL): the roles of monsoon dynamics. *Sci. Rep.* 8, 3960. <https://doi.org/10.1038/s41598-018-22267-z>.
- Mahowald, N., Jickells, T.D., Baker, A.R., Artaxo, P., Benitez-Nelson, C.R., Bergametti, G., Bond, T.C., Chen, Y., Cohen, D.D., Herut, B., Kubilay, N., Losno, R., Luo, C., Maenhaut, W., McGee, K.A., Okin, G.S., Siefert, R.L., Tsukuda, S., 2008. Global distribution of atmospheric phosphorus sources, concentrations and deposition rates, and anthropogenic impacts. *Global Biogeochem. Cycles* 22, GB4026.
- Painter, T.H., Deems, J.S., Belnap, J., Hamlet, A.F., Landry, C.C., Udall, B., 2010. Response of Colorado River runoff to dust radiative forcing in snow. *P. Natl. Acad. Sci. USA* 107, 17125–17130.
- Pope, C.A., Burnett, R.T., Thun, M.J., Calle, E.E., Krewski, D., Ito, K., Thurston, G.D., 2002. Lung cancer, cardiopulmonary mortality, and long-term exposure to fine particulate air pollution. *J. Am. Med. Assoc.* 287, 1132–1141.
- Qian, Y., Gustafson, W.I., Leung, L.R., Ghan, S.J., 2009. Effects of soot-induced snow albedo change on snowpack and hydrological cycle in western United States based on Weather Research and Forecasting chemistry and regional climate simulations. *J. Geophys. Res.* 114, D03108.
- Rienecker, M.M., Suarez, M.J., Gelaro, R., Todling, J.B., Liu, E., Bosilovich, M.G., Schubert, S.D., Takacs, L., Kim, G.-K., Bloom, S., Chen, J., Collins, D., Conaty, A., Silva, A.D., Gu, W., Joiner, J., Koster, R.D., Lucchesi, R., Molod, A., Owens, T., Pawson, S., Pegion, P., Pedder, C.R., Reichle, R., Robertson, F.R., Ruddick, A.G., Sienkiewicz, M., Woollen, J., 2011. MERRA: NASA's Modern-Era retrospective analysis for research and applications. *J. Clim.* 24, 3624–3648.
- Schwartz, J., 1994. Air-pollution and daily mortality—a review and meta analysis. *Environ. Res.* 64, 36–52.
- Stauffer, D.R., Seaman, N.L., 1990. Use of four-dimensional data assimilation in a Limited Area mesoscale model. Part I: experiments with synoptic-scale. *Data Mon. Weather Rev.* 118, 1250–1277.
- Stocks, B.J., Fosberg, M.A., Lynham, T.J., Mearns, L., Wotton, B.M., Yang, Q., Jin, J.Z., Lawrence, K., Hartley, G.R., Mason, J.A., McKenney, D.W., 1998. Climate change and forest fire potential in Russian and Canadian boreal forests. *Clim. Change* 38 (1), 1–13.
- Uno, I., Eguchi, K., Yumimoto, K., Takemura, T., Shimizu, A., Uematsu, M., Liu, Z., Wang, Z., Hara, Y., Sugimoto, N., 2009. Asian dust transported one full circuit around the globe. *Nat. Geosci.* 2, 557–560.
- Wang, H., Rasch, P.J., Easter, R.C., Singh, B., Zhang, R., Ma, P.L., Qian, Y., Beagley, N., 2014. Using an explicit emission tagging method in global modeling of source-receptor relationships for black carbon in the Arctic: variations, Sources and Transport pathways. *J. Geophys. Res. Atmos.* 119, 12888–12909. <https://doi.org/10.1002/2014JD022297>.
- Wiedinmyer, C., Akagi, S.K., Yokelson, R.J., Emmons, L.K., Al-Saadi, J.A., Orlando, J.J., Soja, A.J., 2011. The fire inventory from near (Finn): a high resolution global model to estimate the emissions from open burning. *Geosci. Model Dev. (GMD)* 3, 625–641.
- Xu, C., Ma, Y., Yang, K., You, C., 2018. Tibetan plateau impacts on global dust transport in the upper troposphere. *J. Clim.* 31 (12), 4745–4756.
- Yu, H., Remer, L.A., Chin, M., Bian, H., Kleidman, R., Diehl, T., 2008. A satellite-based assessment of transpacific transport of pollution aerosol. *J. Geophys. Res.* 113, D14S12. <https://doi.org/10.1029/2007JD009349>.
- Yu, H., Remer, L.A., Chin, M., Bian, H., Tan, Q., Yuan, T., Zhang, Y., 2012. Aerosols from overseas rival domestic emissions over north America. *Science* 337, 566–569. <https://doi.org/10.1126/science.1217576>.
- Yu, H., Chin, M., Bian, H., Yuan, T.L., Prospero, J.M., Omar, A.H., Remer, L.A., Winker, D.M., Yang, Y., Zhang, Y., Zhang, Z., 2015. Quantification of trans-Atlantic dust transport from seven-year (2007–2013) record of CALIPSO lidar measurements. *Remote Sens. Environ.* 159, 32–249.
- Zaveri, R.A., Peters, L.K., 1999. A new lumped structure photochemical mechanism for large-scale applications. *J. Geophys. Res.* 104, 30387–30415.
- Zaveri, R.A., Easter, R.C., Fast, J.D., Peters, L.K., 2008. Model for simulating aerosol interactions and chemistry (MOSAIC). *J. Geophys. Res.* 113, D13204.
- Zhao, C., Liu, X., Leung, L.R., Johnson, B., McFarlane, S.A., Gustafson Jr., W.I., Fast, J.D., Easter, R., 2010. The spatial distribution of mineral dust and its shortwave radiative forcing over North Africa: modeling sensitivities to dust emissions and aerosol size treatments. *Atmos. Chem. Phys.* 10, 8821–8838.
- Zhao, C., Liu, X., Leung, L.R., 2012. Impact of the Desert dust on the summer monsoon system over Southwestern North America. *Atmos. Chem. Phys.* 12, 3717–3731.
- Zhao, C., Leung, L.R., Easter, R., Hand, J., Avise, J., 2013a. Characterization of speciated aerosol direct radiative forcing over California. *J. Geophys. Res. Atmos.* 118, 2372–2388. <https://doi.org/10.1029/2012JD018364>.
- Zhao, C., Chen, S., Leung, L.R., Qian, Y., Kok, J.F., Zaveri, R.A., Huang, J., 2013b. Uncertainty in modeling dust mass balance and radiative forcing from size parameterization. *Atmos. Chem. Phys.* 13, 10733–10753.
- Zhao, C., Hu, Z., Qian, Y., Leung, L.R., Huang, J., Huang, M., Jin, J., Flanner, M.G., Zhang, R., Wang, H., Yan, H., Lu, Z., Streets, D.G., 2014. Simulating black carbon and dust and their radiative forcing in seasonal snow: a case study over North China with field campaign measurements. *Atmos. Chem. Phys.* 14, 11475–11491.